

Optic Disk and Macula Detection from Retinal Images using Generalized Motion Pattern

Gaurav Mittal
CVIT IIT-Hyderabad
Email: gaurav.mittal@research.iiit.ac.in

Jayanthi Sivaswamy
CVIT, IIT-Hyderabad
Email: jsivaswamy@iiit.ac.in

Abstract—Accurate detection of optic disk and macula are of interest in automated analysis of retinal images as they are landmarks in retina and their detection aids in assessing the severity of diseases based on the locations of abnormalities relative to these landmarks. The general strategy is to design different methods to these landmarks. In contrast, we propose a novel and unified approach for Optic disk and macula detection in this paper using the Generalized Motion Pattern (GMP) [10] [19] which is derived by inducing motion to an image to smooth out unwanted information. The proposed method is unsupervised, parallelizable and handles illumination differences efficiently but assumes a fixed protocol in image acquisition. The proposed method has been tested on five public datasets and obtained results indicate comparable performance to supervised approaches for the same problem.

I. INTRODUCTION

Early diagnosis and timely treatment can prevent up to 98% of severe vision loss in sight threatening diseases like Diabetic retinopathy and Glaucoma etc. Digital images of the retina acquired with or without pupil dilation, is used for screening such diseases and their automated analysis has received much attention in last two decades [13]. Accurate detection of important landmarks, namely, the optic disk (OD) and macula is useful in many ways: The OD location is useful to boost the bright lesion detection performance of CAD algorithms, as OD share many visual characteristics with bright lesions. The location of OD and macula aids in determining the severity of the disease and need for intervention. For instance, the proximity of a bright/dark lesion to macula indicates a higher likelihood of impaired vision and hence calls for immediate medical attention. Such precise location is also needed in registering images acquired across patient visits and assessing disease progression. In general the detection of OD and macula from colour retinal images has been treated as two separate problems, with OD detection receiving more attention than macula detection. OD detection methods typically exploit the appearance info. such as colour and roughly circular shape.

While some early attempts relied only on luminosity in the green channel, their failure in the presence of other bright lesions quickly gave rise to supervised methods. Supervised methods such as [4] [14] aims at learning the structure and luminosity distribution of OD. The performance of these methods rely on good training and test images and fixed protocol (same magnification, resolution etc.) imaging. Their performance tend to degrade on new datasets/unseen images. The roughly round shape of OD geometric modelling has also been attempted in its detection via Hough transform [16]. In

addition to the high computational cost of the transform, the model fails in images with poor illumination (due to small pupil size) which renders uncertainty in the boundary between Optic disk and background. Some other approaches to OD detection include those based on vessel crossing information [7], clustering [8], regression [12], projections along multiple directions [15] and a joint detection of macula and OD [6]. All these methods shows different robustness to the presence of pathologies, uneven illumination etc.

Macula detection has received relatively less attention. A common approach is to use location of detected OD for narrowing down search space [11] [5]. Regression has also been used in determining the location of macula [12]. Recently some joint detection methods [6] have been proposed, which detects both OD and macula simultaneously.

We aim to detect OD and macula using a unified approach which uses the concept of Generalized Motion Pattern (GMP) that was introduced in [10] and demonstrated for global detection of abnormalities from mammograms and retinal images. The GMP is derived by inducing motion to an image, which serves to smooth out unwanted information while highlighting the structures of interest. This concept was extended in [19] by inducing a set of motions to a given image and combining the results to construct an *Interference map*. This map was demonstrated to be useful in building an assistive tool for local lesion annotations. In this paper we demonstrate how this concept of interference map can be applied to the problem at hand: OD and macula detection.

The main contribution of this paper is an unsupervised, parallelizable OD and macula detection algorithm for fixed protocol DR datasets. The method is highly robust to uneven illumination and small pathologies. Our method does not require much parameter tuning and we have used same set of parameters for all the 5 public datasets we reported the results on, which is another big contribution.

Rest of the paper is organized as follows: Section II summarises the concept of GMP and interference map. Section III and IV presents the proposed approach for OD and macula detection, respectively. Section V explains the experiments done and also reports results on several public data-sets. Final conclusion and scope for future work is given in section VI.

II. GMP AND INTERFERENCE MAP

Given an gray scale image I , its GMP representation I_{GMP} [10] is defined as

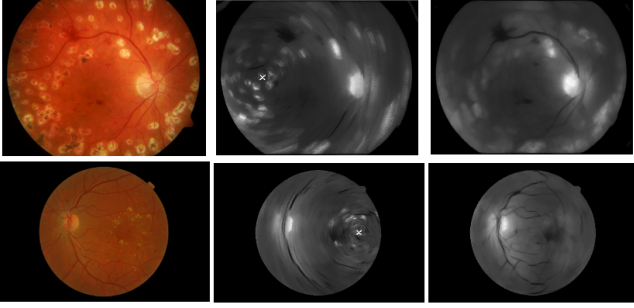


Fig. 1. GMP and interference map for samples images from Directdb (top row) and Messidor (bottom row). From left to right: original image, GMP about the pivot shown as white cross and interference map.

$$I_{GMP}(\vec{r}) = f(I(T_j(\vec{r})|1 \leq j \leq N)) \quad (1)$$

Here \vec{r} denotes the pixel location, $T_j(1 \leq j \leq N)$ denotes j^{th} rigid transformation applied to I which produces j^{th} resultant image. Total N images are produced and these images are combined into the GMP map using a coalescing function $f(\cdot)$. $f(\cdot)$ maps the set of pixel intensities at each location (\vec{r}) across the transformed images to a scalar value.

GMP interference map generation: The combination of a family of GMPs generated by inducing rotation motion in a given image is defined as an interference map [19]. For a given image I , let the GMP with rotation about a pivot P_k be I_{GMP}^k . An ensemble of K GMPs is generated when K pivot points are chosen: $C_K = \{I_{GMP}^k|1 \leq k \leq K\}$. The interference map I_{int} is generated from C_K as follows

$$I_{int}(\vec{r}) = \phi(C_K) = \phi(\{I_{GMP}^k(\vec{r})|1 \leq k \leq K\}) \quad (2)$$

where $\phi(\cdot)$ maps the ensemble of GMPs to a single map.

In our work, each I_{GMP}^k was generated using eq. 1, with T as rotation by an angle in the range $(-\theta, \theta)$ degrees in steps of 1 degree. The coalescing function $f(\cdot)$ was chosen as median. The rotation range $(-\theta, \theta)$ controls the degree of rotational motion. $\phi(\cdot)$ was chosen to be a pointwise quartile generator which generates quartile intensity value for $I_{int}(\vec{r})$ from GMPs with $K = 150$ randomly chosen pivot points. Fig. 1 shows two sample images and their corresponding GMP (only one) and the final interference map. The blur seen in the GMP is due to the induced rotational motion. The interference map is seen to effectively localise OD as a bright region, while suppressing minor vessels and the bright circular artifacts (due to laser surgery). This is also notwithstanding the poor illumination.

III. OPTIC DISK DETECTION USING INTERFERENCE MAP

Our OD detection pipeline consists of two major stages. Stage one is candidate selection which is based on interference map and stage two is candidate rejection which is based on domain knowledge-based cues.

A. Optic disk candidate selection

The optic disk candidate selection is based on an observation from the I_{int} , that the intensity value in the OD region is higher than background and the intensity value decreases as we move away from OD center.

Optic disk candidates are obtained from a series of j binary maps where I_{bin}^j obtained as follows.

$$I_{bin}^j(\vec{r}) = \begin{cases} 1 & \text{if } I_{int}(\vec{r}) > I_{high} - j * step_size \\ 0 & \text{otherwise} \end{cases} \quad (3)$$

$$step_size = (I_{high} - I_{low})/20 \quad (4)$$

where I_{high}/I_{low} are the highest/lowest intensity value of I_{int} and j is from 1 to 6.

Note that I_{bin}^1 binary image will have lowest number of candidate regions, while I_{bin}^6 will have maximum. The geometric center of the candidate region in I_{bin}^j with the lowest j index is taken as the candidate OD center. It is worthwhile to note that in 75-80% of retinal images, there is only one candidate point passed by this stage. However, to handle the cases with multiple candidates (due to pathologies or artifacts) a rejection scheme is required which is described next.

B. Determining the final optic disk location

Three, rule-based, unsupervised, rejection stages are designed to determine the final OD center. The first 2 rejection stages are based on vessel and vesselness information which is computed using [20]. The 3rd rejection stage uses previously detected OD position information and assumes a fixed protocol across images, which is generally true in image acquisition for a specific dataset.

1) *Rejection based on vessel direction:* This rejection stage is based on the observation that near OD, the direction of vessels is vertical. This rejection stage gives good horizontal localization by rejecting candidates caused by bright lesions. The sum of horizontal gradients on the vessel tree around candidate points is found in a $m \times n$ rectangular box with $m = 2n$. This sum is thresholded to perform the rejection.

2) *Rejection using vesselness:* OD is bright region where vessels exit the retina so candidates that do not enclose vessels can be rejected. This is done by computing the vesselness (the probability of a pixel being the part of a vessel). The sum of vesselness values in a square region around a candidate is found and thresholded to reject false candidates which typically occur in the bright regions above and below the OD.

3) *Rejection using expected OD location:* This stage assumes that a fixed protocol has been used for image acquisition, which is generally true. Fixed protocol limits the possible locations where OD is highly likely to be found in a given image. This can be found offline, using the ground truth. We used an alternate method using a 2-pass strategy where all the images with single detected candidate for OD were used to find the set of possible OD locations $S : \{\vec{r}_n\}$. By clustering \vec{r}_n values, S is partitioned into 2 subsets, one each, for the left and right eye. These subsets aid defining the mean OD locations for the right and left eyes: \vec{r}_R and \vec{r}_L , for a given dataset. In the 2nd pass, images with multiple candidates were processed using the distance of candidates to \vec{r}_R and \vec{r}_L , to retain the candidate with minimum distance as final OD center.

Fig. 2 shows a sample image and its computed I_{int} where 5 candidates were found. The OD region is not well delineated in I_{int} as there is also a bright region below it. Nevertheless, the 3 rejection stages successfully eliminate the false candidates

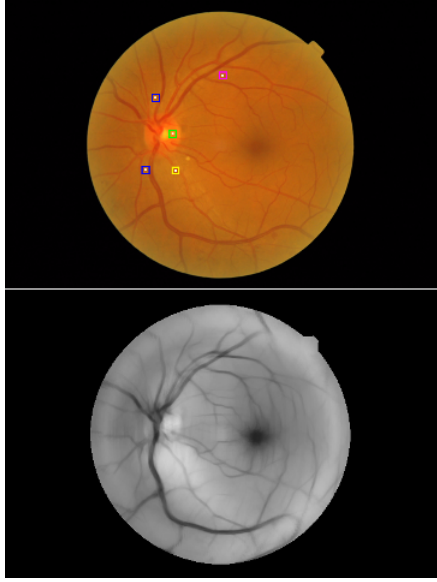


Fig. 2. Example image and respective interference map with candidate points shown as white dots. Pink, yellow and blue squares represents rejection because of stage 1,2,3 respectively. Final detected OD is surrounded by green square.

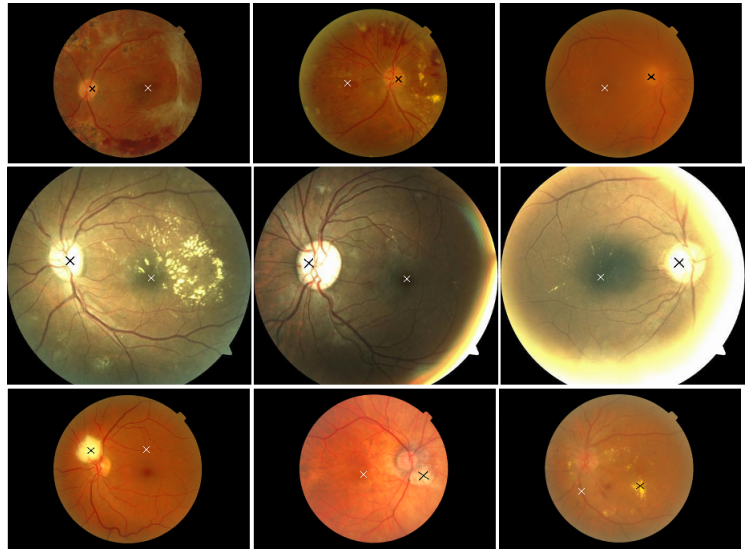


Fig. 3. OD and macula detection results (Black cross represents OD and white cross represents macula). Top two rows show correct detections in images from Messidor and DMED, respectively. Last row shows failure cases (from left to right) due to image capture, failure in rejection stages and presence of large pathologies.

(1 each by the first two stages and 2 by the third stage) and retain the correct candidate (in green box).

IV. MACULA DETECTION USING DETECTED OPTIC DISK

It is a clinical fact that the distance of macula center from optic disk center is roughly 2.5 times diameter of the OD. It appears as a dark region bereft of vessels. In this work, we use the computed position of OD to narrow down the search space for macula detection. Determining the accurate OD radius for each image is a very challenging task so instead of defining the macula search space in terms of OD radius, we define it as a ratio of image FOV (the circular bound of the image) radius with respect to detected OD location r_{OD} . Since the relation between OD radius and image FOV radius depends on image magnification, this search space is slightly different for each dataset. However, in our experiments it was observed this variation is negligible and general parameters can be used.

Since macula is the darkest region locally, the green plane of macula search space of the given image (I_{sub}) is processed to generate several binary images using multiple thresholding. The idea here is similar to the one we followed for OD candidate generation.

$$I_{bin}^k(\vec{r}) = \begin{cases} 1 & \text{if } I_{sub}(\vec{r}) < I_{low} + k \times step_size \\ 0 & \text{otherwise} \end{cases} \quad (5)$$

Here I_{sub} is cropped sub-image and I_{low} is lowest intensity in sub-image. In our implementation, $k = 1 : 10$ and $step_size = (I_{high} - I_{low})/20$, which means that we are assuming that fovea lies in the bottom 50% intensity range and its center is darker than its surroundings. These parameters ensure adaptation to an image and hence robustness across datasets.

After generating multiple binary images macula center candidates are generated in a similar manner as OD candidates.

In rare cases where there are multiple candidates, the candidate closest to sub-image I_{sub} center is chosen as the macula center.

V. RESULTS AND EXPERIMENTS

The proposed method was evaluated on 5 public datasets including Messidor [2], Diaret-db0&-db1 [17], [18], DMED [1] and DRIVE [9], out of which only DRIVE had OD and macula markings available. Annotations for other datasets were obtained locally. OD was marked as an elliptical disk and macula center was marked as a point. OD was marked on all the images and since the macula location is not clear in some images, those images were skipped during macula marking.

Messidor dataset has 1200 high resolution images out of which first 800 images are pupil dilated. First 800 images from Messidor, all 130 images from Diaretdb0, all 89 images from Diaretdb1 and all 169 images from DMED were marked for OD and macula. All of these datasets has significant variance in terms of abnormality distribution, brightness, illumination etc. Within each dataset FOV and magnification is similar and all of these datasets are macula centered.

Table I reports the results for OD detection and OD localization accuracy. OD is considered to be correctly detected if the detected OD lies within the marked elliptical OD boundary. We also report localization accuracy in terms of distance from center of OD, normalized by mean OD radius R which is calculated for each dataset using marked elliptical boundary. Our method has good localization accuracy because OD center is characterized by high intensity values in I_{int} .

Table II compare our method with other recent works. As we can observe, our method consistently outperforms the unsupervised algorithm [3] and is comparable in perform with ensemble based supervised technique [6]. Here '-' signifies that the method did not report result on that particular dataset.

Results Dataset name	Optic disk				
	Accuracy	% images within (R is avg. OD radius)			
		$R/4$	$R/2$	R	$2R$
Messidor(first 400)	98.50	84.25	98.5	99	99.5
Messidor(400 - 800)	98.25	85.25	98	99	99.75
Directdb0(130 images)	96.15	82.31	96.92	97.69	98.46
Directdb1(89 images)	95.51	82.02	94.38	97.75	97.75
DMED(169 images)	97.04	86.39	96.44	97.04	98.81
DRIVE (40 images)	100	60	100	100	100

TABLE I. RESULTS FOR OPTIC DISK DETECTION

Method	Messidor	Directdb0	Directdb1	DMED	Drive
[14] Supervised	-	98.50	97.75	-	97.5
[3] Unsupervised	97.80	86.50	86.50	-	97.5
[21] Supervised	-	97.0	96.20	-	100
[6] Supervised and Ensemble	-	97.64	97.79	-	100
Proposed Unsupervised	98.50	96.15	95.51	97.04	100

TABLE II. COMPARISON OF DETECTION RATES FOR OD

Only those images, where macula position is clearly visible were marked during local data annotation. We show macula detection results on both local [2], [17], [18], [1] and publicly available [9] markings. Macula detection results are presented in Table III. [4] reports detection accuracy of 98.24% on locally marked marked 1136(out of 1200) images of Messidor and accuracy of 94.38% on Direct-db1. Their accuracy is slightly higher for messidor but lower for Direct-db1 compared to our method.

Our method performs better for OD detection as compared to macula detection, because macula detection is a harder problem and it's result depends upon accurate OD results, as OD position is used to limit it's search space. Qualitative results for some images are also shown in Fig. 3.

The interference map is computed on green channel of illumination corrected image after fundus extension (FOV extension). Creating GMP for an image size of $R \times C$ has computation complexity of $O(R \times C \times \theta \times N)$, as we need to perform $O(\theta \times N)$ image rotation operations. In our work angle range is $(-7, 7)$, number of pivot points are 150 and R, C are number of rows and columns of image respectively. Because of this GMP computations becomes very slow for high resolution images. To speed up computation, all the images were resized to 640 rows while preserving aspect ratio because candidate selection is relatively unaffected by resolution reduction as GMP suppresses local information and this also permits the use of a fixed set of theta range and pivot points N values across datasets.

GMP interference map creation takes 2-3 minutes on a unoptimized, single threaded Matlab code running on Ubuntu with 2.1 GHz processor and 4 GB RAM. After computing GMP interference map, rest of the stages takes 2-3 seconds for computing OD and macula center.

Dataset name	Messidor		Direct		DMED	Drive
	First 400	400-800	db0	db1		
Marked images	340/400	343/400	81/130	58/89	145/169	37/40
Proposed Accuracy	97.5	98	95.85	96	96.44	100

TABLE III. DETECTION RATES FOR MACULA ON POPULAR DATASETS

CONCLUSION

In this work we have used the Generalized motion pattern concept from [10] and [19] and modified it for OD and macula detection. We have tested our algorithm on various public datasets and showed that our method performs better than other unsupervised algorithms. Our method does not require much tuning of parameters across datasets. In the current implementation, the bottleneck is in interference map creation. Since this is highly parallelizable, it can be explored in the future.

REFERENCES

- [1] Kindly provided by the DMED program partners (see <http://vibot.u-bourgogne.fr/luca/heimed.php>).
- [2] Kindly provided by the messidor program partners (see <http://messidor.crihan.fr>).
- [3] M. I. Ahmed et al. High speed detection of optical disc in retinal fundus image. *Signal, Image and Video Processing*, pages 77–85, 2015.
- [4] A. Aquino et al. Establishing the macular grading grid by means of fovea centre detection using anatomical-based and visual-based features. *Computers in Biology and Medicine, Science direct*, 2014.
- [5] A. D Fleming et al. Automated Assessment of Diabetic Retinal Image Quality Based on Clarity and Field Definition. *Investigative Ophthalmology and Visual Science*, pages 1120–1125, 2006.
- [6] A Giachetti et al. Combining algorithms for automatic detection of optic disc and macula in fundus images. *Computer Vision and Image Understanding*, pages 138–145, 2012.
- [7] Aliaa Abdel Haleim et al. Optic disc detection from normalized digital fundus images by means of a vessels direction matched filter. *IEEE Transactions on Medical Imaging*, 2008.
- [8] H. Li et al. Automatic location of optic disk in retinal images. *International conf on image processing*, pages 837–840, 2001.
- [9] J.J. Staal et al. Ridge based vessel segmentation in color images of the retina. *IEEE Transactions on Medical Imaging*, 2004.
- [10] K. Sai Deepak et al. Automatic Assessment of Macular Edema From Color Retinal Images. *IEEE Transactions on medical imaging*, 2012.
- [11] M. E. Gegundez-Arias et al. Locating the fovea center position in digital fundus images using thresholding and feature extraction techniques. *Computerized Medical Imaging and Graphics*, pages 386–393, 2013.
- [12] M. N. Michael et al. Fast detection of the optic disc and fovea in color fundus photographs. *Medical image analysis*, pages 859–870, 2009.
- [13] Oliver Faust et al. Algorithms for the Automated Detection of Diabetic Retinopathy Using Digital Fundus Images: A Review. *Journal of Medical Systems*, 36:145–157, 2012.
- [14] S. A. Ramakanth et al. OD-Match: patchmatch based optic disk detection. *Fourth National Conference NCVPRIPG*, pages 1–4, 2013.
- [15] S. Lu et al. Automatic optic disc detection from retinal images by a line operator. *IEEE Transactions on Biomedical Engineering*, 2011.
- [16] S. S. Waleed et al. Automated localisation of retinal optic disk using hough transform. *Biomedical Imaging: From Nano to Macro, IEEE ISBI*, 2008.
- [17] T. Kauppi et al. DIARETDB0: Evaluation database and methodology for diabetic retinopathy algos. *Machine Vision and Pattern Recognition Research Group, Lappeenranta University of Technology*, 2006.
- [18] T. Kauppi et al. The DIARETDB1 Diabetic Retinopathy Database and Evaluation Protocol. *British Machine Vision Conference*, 2007.
- [19] Ujjwal et al. An assistive annotation system for retinal images. *IEEE International Symposium on Biomedical Imaging*, 2015.
- [20] A F Frangi. Multiscale vessel enhancement filtering. *Medical Image Computing and Computer-Assisted Intervention MICCAI*, pages 130–137, 1998.
- [21] A. Tewari and J. Sivaswamy. Bilateral Symmetry Based Approach for Joint Detection of Landmarks in Retinal Images. *International Conference on Signal Processing and Communications*, 2014.